Mausam, (1985), **36**, 3, 275-286

551.553 : 551.553.21(266)

Barotropic instability over the Arabian Sea during the onset of summer monsoon 1979

SOON-UNG PARK

Dept. of Meteorology, College of Natural Sciences, Seoul National University, Seoul, 151, Korea

and

DHIRENDRA N. SIKDAR

Atmospheric Sciences, University of Wisconsin-Milwaukee, Milwaukee, Wisconsin 53201, *USA*

(*Received 3 February 1984*)

सार — 1979 में ग्रीष्म कालीन मानसून की आरम्भिक अवस्थाओं के लिए 26° उत्तर से 16° दक्षिण तक तथा 30° पूर्व से 84° पूर्व तक के क्षेत्र में अरब सागर के ऊपर देखी गई दैनिक निम्नस्तरीय तथा उच्च स्तरीय उपग्रह पवनों का विश्लेषण किया गया है। पवनों के विलेश्षण से पता चलता है कि दक्षिण भारत में मानसून शुरू होने से पहले निम्न स्तरीय पवनें उल्लेखनीय रूप से प्रबल होती हैं। मानसून आरंभ होने पर भ्रमिल बनता है तथा निम्नस्तरीय पछुआ जेट उत्तर की ओर चला जाता है तथा मध्यवर्ती अरब सागर में जाकर फैल जाता है। मानसून आरंभ होने से पूर्व की अवस्था, भ्रमिल निर्माण, मानसून आरंभ होना तथा उसकी प्रकृति के लिये क्षेत्रीय पवनों का आंकिक रूप से एक रेखीय दाबघनत्व विश्लेषण किया गया था। इसके द्वारा इन परिकल्पनाओं का परीक्षण किया गया था : (1) मानसून के आरंभ में भ्रमिल का निर्माण उस तरंग विक्षुब्धता के कारण होता है जो मध्य क्षेत्रीय अपरूपण प्रवाह में दाबघनत्व अस्थायित्व से संबंधित है तथा (2) निम्नस्तरीय जैट का फैलना आंशिक रूप से दाबघनत्व तरंग विक्षुब्धता के गतिकीय परिणामों के कारण होता है।

दाब घनत्व अस्थायित्व के लिये आवश्यक स्थितियां मानसून आने से पहले तथा भ्रमिल निर्माण के बीच की अवधि में स्तरीय प्रवाहों में तो मिल जाती है / पूरी हो जाती है किन्तु मानसून आ जाने के बाद की अवधि में नहीं मिल पाती तथापि ऊपरी स्तर पर दाबघनत्व अस्थायित्व के लिये आवश्यक स्थितियां नहीं मिल पातीं। इन प्रेक्षणों से पता चलता है कि केवल ग्रीष्मकालीन मानसून की आरंभिक अवस्थाओं में ही अरब सागर के ऊपर दाबघनत्व अस्थायित्व महत्वपूर्ण है और यह केवल निचले क्षोभमण्डल तक ही सीमित है। दाबघनत्व अस्थायित्व चित्र मानसून पूर्व अवस्था में बहुविध तरंग विक्षुब्धताओं की तथा भ्रमिल निर्माण अवस्था में एक प्रमुख विध (वेवलैन्थ $\simeq$2000 कि. मी.) की उपस्थिति दर्शाते हैं। दोनों ही अवस्थाओं में 2000 कि. मी. वाले विध (Mode) की विकास दर अधिकतम है तथा यह मोटेतौर पर मानसून के आंरभ में बने भ्रमिल, जैसा कि उपग्रह से प्राप्त चित्रों में दिखाई देता है, के आकार पर निर्भर करता है। दाबघनत्व तरंग विक्षुब्धता दक्षिणपश्चिम से उत्तरपूर्व की ओर सरक जाती है। जिसके कारण पछुआ पवन संवेग उत्तर की ओर बढ़ जाता है। अधिकतम क्षेत्रीय अपरूपण क्षेत्र के एकदम उत्तर में बढ़े कुल संवेग के कारण अरब सागर के ऊपर निम्न स्तरीय जेट के प्रवाह की गति बढ़ सकती है तथा वह विस्तृत हो सकता है।

ABSTRACT. The daily low-level and upper-level satellite winds observed over the Arabian Sea in the domain 26°N-16°S and 40°E-84°E are analyzed for the early stages of the summer monsoon in 1979. The wind analysis shows that before the onset of the monsoon over southern India, the low-level winds strengthen significantly, an onset vortex develops, and the low-level westerly jet shifts northward and broadens in the central Arabian Sea. A linear barotropic stability analysis of the zonal winds for the pre-onset, the vortex formation, the onset and the mature phases of monsoon flows is performed numerically for testing the hypothesis that the onset vortex formation is primarily due to the wave disturbances associated with barotropic instability in the mean zonal shear flow, and that the broadening of the low-level jet is partly due to dynamical consequences of the barotropic wave disturbances.

The necessary condition for barotropic instability is satisfied in the low-level flows during the pre-onset and the vortex formation periods but barely for the onset phase. At upper levels, however, the necessary condition for barotropic instability is not satisfied. These observations suggest that barotropic instability is important only during the early phases of the summer monsoon over the Arabian Sea, and is confined to the lower troposphere. Barotropic stability diagrams reveal the existence of multimode wave disturbances in the pre-onset phase, and one dominant mode (wavelength $\simeq$ 2000 km) in the vortex formation phase. In both stage the 2000 km mode has the maximum growth rate, and roughly corresponds to the size of the onset vortex as seen in the satellite pictures. The barotropic wave disturbance tilts southwest to northeast implying a northward transport of the westerly momentum. The net gain of momentum just north of the maximum zonal shear zone may be responsible for an acceleration of the flow and the broadening of the low-level jet over the Arabian Sea.

1. Introduction

During the Summer Monsoon Experiment (MONEX) period (1 May to 31 July 1979) an excellent set of stallite winds was produced from GOES-I satellite time lapse imagery over the Indian Ocean. This data set gave meteorologists the first opportunity to observe from space the genesis of the monsoon circulation over the Arabian Sea. A central problem in MONEX is the understanding of the regional aspects of the onset of monsoon rains. This paper is an attempt to understand the

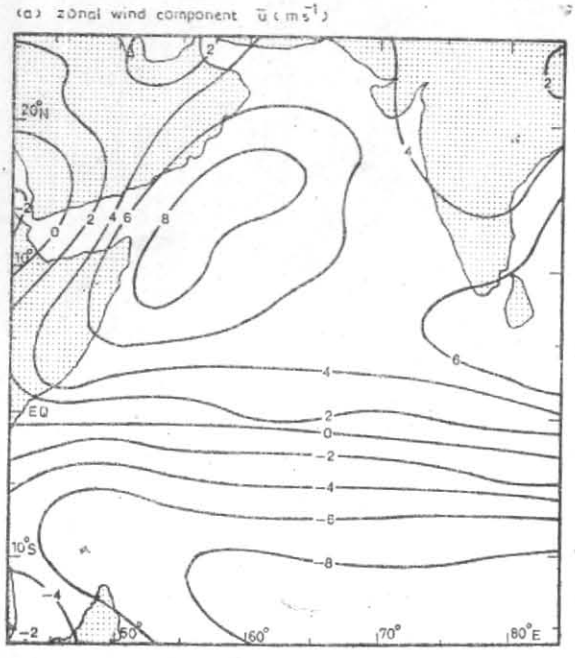

Fig. 1. The distribution of low-level zonal wind component $\bar{u}$ (ms^{-1}) averaged for two months (May and June 1979)

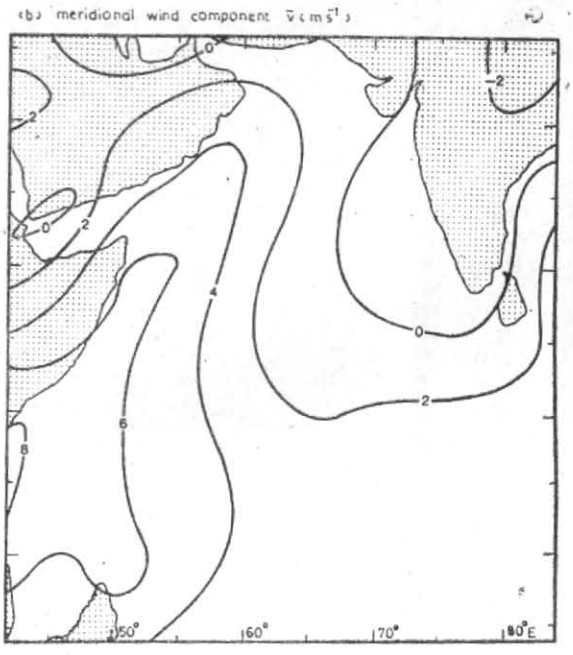

Fig. 2. As in Fig. 1 except for the meridional wind component $\bar{v}$ (ms^{-1}).

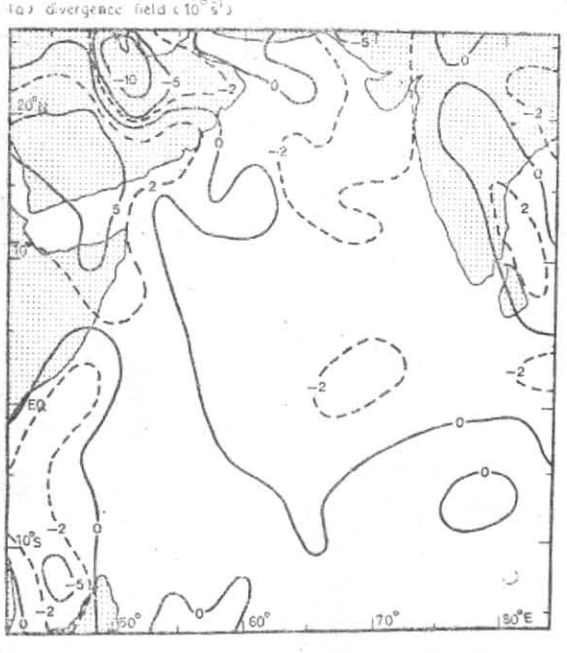

Fig. 3. The two-month mean low-level divergence field (10^{-6}s^{-1})

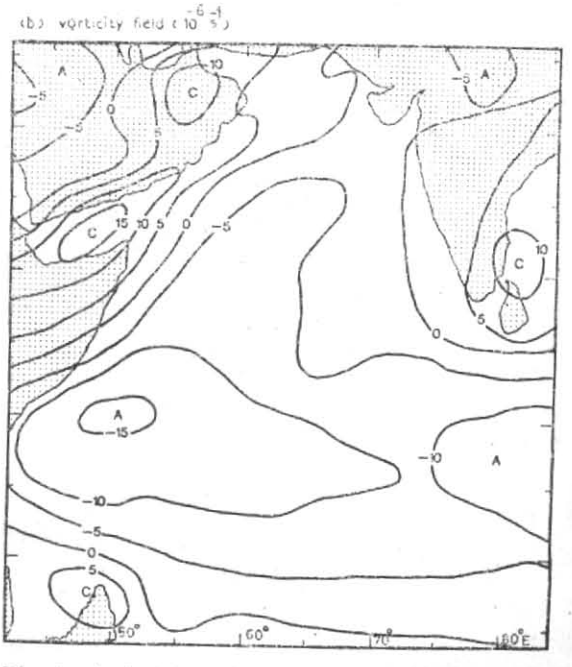

Fig. 4. As in Fig. 3 except for the vorticity field (10^{-6}s^{-1}). The letters A and C represent the primary centres of the anticyclonic and cyclonic vorticity respectively

dynamic mechanisms involved in the initiation of monsoon onset over the Arabian Sea.

The wind analyses suggest that the horizontal shear of the monsoon current changes substantially during the monsoon onset. Krishnamurti *et al.* (1981) showed a substantial temporal variation in the growth rate of barotropically unstable waves during the formation of the onset vortex, based on the computation of growth rate for each day using daily zonal winds. However, analysis is questionable since the daily basic zonal wind used in their model is not time independent during the growth of an unstable mode.

The monsoon onset is a spectacular event. During the 1979 monsoon onset period, the strengthening of the westerlies on its equatorward side is followed by an onset vortex in the eastern Arabian Sea, and the beginning of rain on the west coast of India. Once the monsoon has set in over the Indian subcontinent, a widespread heavy precipitation is a common feature, and the latent heat released plays a dominant role in the monsoon dymnaics. Shukla (1978) concluded that monsoon depressions over the Bay of Bengal are triggered by barotropic instability but their sustenance and amplification are accomplished by latent heat of condensation. This probably implies that different dynamic mechanisms are involved at different stages of the monsoon circulation.

The stability of barotropic zonal currents with respect to wave disturbances has been studied by Kuo (1949, 1973), Eliassen (1954), Lipps (1962, 1965), Yanai and Nitta (1968) and others. They found a necessary condition for barotropic instability in a hypothetical zonal current. Barotropic instability plays an important role on the synoptic scale disturbances in the tropical Pacific (Riehl 1948; Bates 1970). However the role of barotropic instability in the monsoon circulation has not been satisfactorily examined. The questions that will be addressed to in this paper include: Is barotropic instability important in the onset phase of the summer monsoon ? If so, does it continue to play a major role during the mature phase of the monsoon ?

Charney (1963) indicated that in the absence of condensation the large-scale motions in the tropics tend to be quasi-horizontal and quasi-nondivergent. This may be true for early stages of the monsoon. We will not consider the mature stage of the monsoon (July and August), since we believe that the control centre of monsoon rain shifts to the Bay of Bengal during this period and that the well organized monsoon disturbances are maintained by the Conditional Instability of the Second Kind (CISK) as found in the tropical regions (Yamaski 1969; Kuo 1965; Charney and Eliassen 1964; Bates 1970; Williams *et al.* 1971).

2. Data analysis techniques

The data used in this study are the set of satellite winds analyzed at the University of Wisconsin for the summer MONEX in 1979. The original data covered the region between 40° N and 40° S latitudes and 30° E and 110°E longitudes for three months (May, June, July) at two levels ; the lower layer at about 850 mb and the upper layer at about 200 mb. All data were interpolated to a $2° \times 2°$ grid using the objective analysis scheme developed by Endlich and Mancuso (1968). Further details are available in the Summer Monsoon Windsets from Geostationary Satellite Data (Young *et al.* 1980).

The low-level and the upper-level winds were averaged over May and June at each grid point in the domain between 28° N and 18° S latitudes and 40° E to 84° E longitudes. From these averaged data the horizontal divergence $\frac{\partial \bar{u}}{\partial x} + \frac{\partial \bar{v}}{\partial y}$ and the vertical component of vorticity, $\frac{\partial \bar{v}}{\partial x} - \frac{\partial \bar{u}}{\partial y}$ are calculated at each mesh point where x and y and directed toward the east and north respectively. In calculating the vorticity and the divergence we have used the horizontal coordinates in the mercator projection. In the following sections we present satellite wind analyses.

3. Low-level flow field

Figs. 1 and 2 show the two-month mean low-level $\bar{u}$ and $\bar{v}$ components respectively. The easterlies (Fig. 1) are confined in the Southern Hemisphere while the westerlies dominate in the Northern Hemisphere. Near the coast of Somalia a well defined low-level wind maximum zone (known as the Somali jet or the east African jet) extends from the equator northeastward over the Arabian Sea. There is a zone of strong westerly wind near extreme southern India. A strong southerly wind in Fig. 2 extends northeastward from the east coast of South Africa in the Southern Hemisphere into the Arabian Sea, while a weak northerly wind prevails over the Indian subcontinent.

The low-level divergence and relative vorticity fields are presented in Figs. 3 and 4 respectively. Maximum values of divergence of about $8 \times 10^{-6} s^{-1}$ are found over Saudi Arabia. A weak divergence is found in Somalia and in the southern part of India, and a wide area of convergence is seen in the Arabian Sea, the east coast of South Africa, and the eastern part of India. A narrow region of strong convergence is seen over northern parts of Saudi Arabia (Fig. 3). In the mean voriticity field in Fig. 4 the most outstanding feature is the presence of a prominent anticyclonic vorticity centred along the equator, which extends northeastward into the Arabian Sea. A cyclonic vorticity is found in the western Arabian Sea and Saudi Arabia. The cyclonic vorticity is separated from the anticyclonic vorticity by a Somali jet extending northeastward from the coast of Somalia near the equator. Over India the cyclonic vorticity is present with maximum values in the eastern part of India, where relative maximum divergence is noticed. The magnitude of the vorticity is at places roughly one order of magnitude larger than that of the divergence.

4. Upper-level flow field

Two-month mean upper level $\bar{u}$ and $\bar{v}$ components are illustrated in Figs. 5(a & b) respectively. The upper level easterlies (Fig. 5a) occupy a broad area of the Arabian Sea and the southern Indian Ocean from 20° N to 10°S with maximum wind zones over the western Arabian Sea along the coastline and the southern tip of India. The location of upper level-easterly maximum broadly

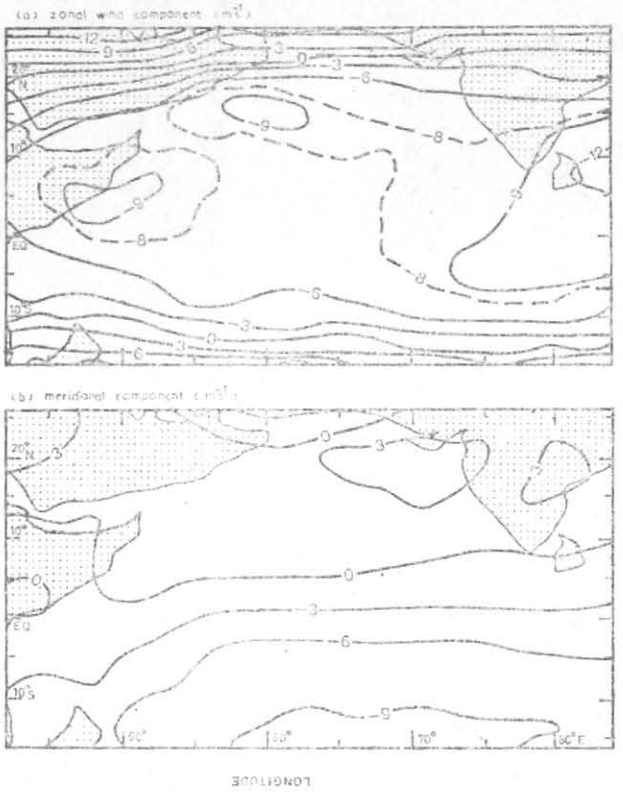

Fig. 5. The distribution of upper-level (a) zonal wind component (ms $^{-1}$) and (b) meridional component (ms^{-1} (averaged for two months (May and June 1979)

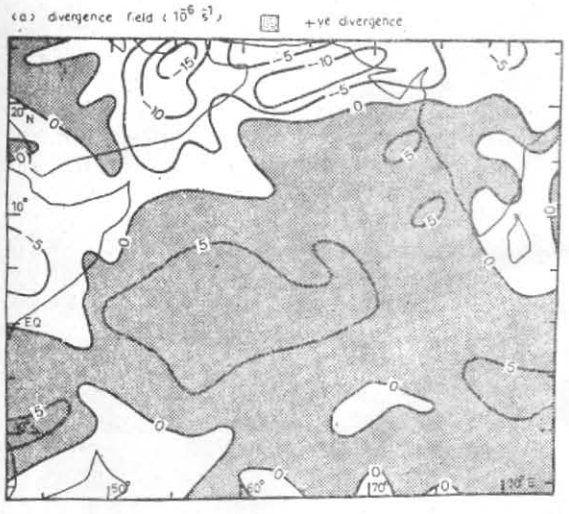

Fig. 6. The two-month mean upper-level divergence field ($10^{-6}s^{-1}$). The shaded area represents positive divergence

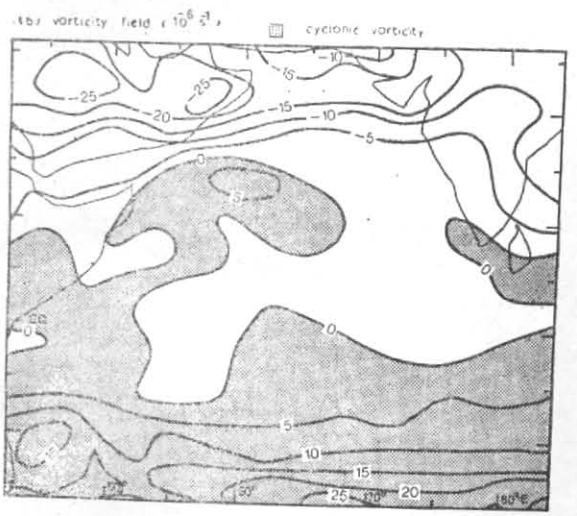

Fig. 7. As in Fig. 6 except for the vorticity field ($10^{-6}s^{-1}$). The shaded area represents the cyclonic vorticity

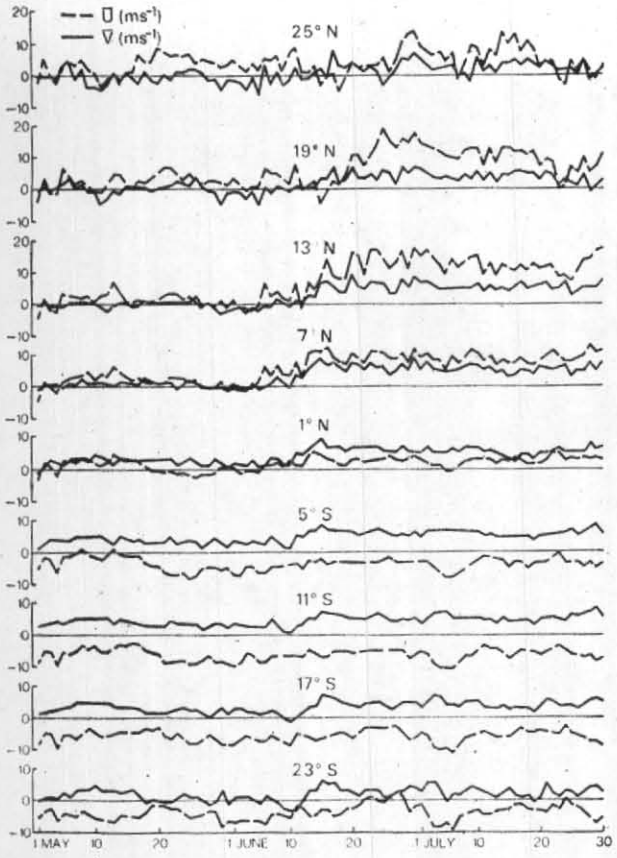

Fig. 8. Time sections of zonal wind (.....) and meridional wind (——) components averaged over 6° of latitude and over 40°E-84°E-longitude for three-month (May, June and July 1979) period

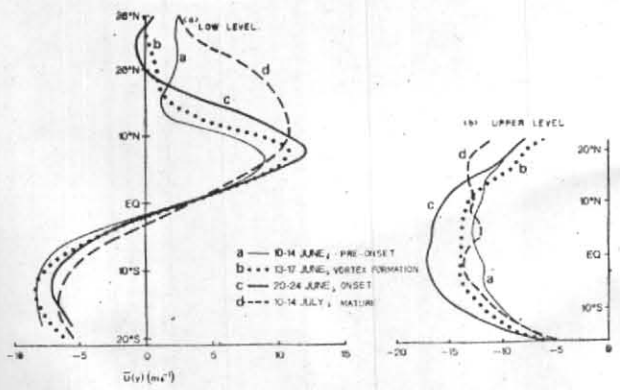

Fig. 9 Fig. 10

Figs. 9 & 10. Meridional profiles of (Fig. 9) low-level mean zonal winds and (Fig. 10) upper-level zonal winds averaged over 40° E–84°E longitude for : a- the pre-onset (——), b- the vortex formation (...), c- the onset (——) and d- the mature (. . . .) phases. The profiles extend from 22°N to 16° S.

coincides with that of the westerly maximum at lower level. The meridional wind pattern in Fig. 5(b) shows a southerly flow north of 5° N and a northerly flow to the south with a maximum around 16° S (not shown). The cross equatorial flow appears weak compared to that in the low-level (Fig. 2).

The upper-level mean divergence and relative vorticity are presented in Figs. 6 and 7 respectively. A broad region of divergence dominates most of the Arabian Sea and the southern Indian Ocean with a maximum near the equator, while a strong convergence is found over the northern Arabian Sea, the Arabian desert and Somalia. The vorticity field in Fig. 7 shows that a positive vorticity is confined to the south of the equator and also on the cyclonic shear side of the easterly wind maximum zone extending along the east coast of Somalia into the Arabian Sea. A strong anticyclonic vorticity field dominates north of 15° N with a maximum centred over the Saudi Arabian desert. The observed divergence fields (Figs. 3 and 6) imply that the sinking motion takes place over the western part of the Arabian Sea and the southeastern part of Indian Peninsula while most of the Arabian Sea is dominated by rising motion.

5. Time sections

To examine the evolution of the wind fields with the progression of the monsoon we have constructed time sections of the low-level $\bar{u}$ and $\bar{v}$ components averged over 6° latitude intervals in the longitude span 40° to 84°E for the 3-month periods (Fig. 8). The interesting feature in the pre-onset phase (10-14 June) is the intensification of the zonal and meridional winds progressively in time in the Northern Hemisphere, beginning at the equator around 10 June. In the Southern Hemisphere such significant progression of winds in time is not clear but the strengthening of winds occurs around 10 June in all latitudes. The cross equatorial flow (southerly wind) in the pre-onset phase is also intensified in low latitudes.

The time series are subdivided into serveral different time periods according to the different events associated with the monsoon. Fig. 9 shows the meridional distribution of the time-averaged low-level zonal mean wind over the longitude span 40°-84° E derived from the original data (2° intervals) for the periods of 10-14 June (zonal wind intensification period, Fig. 9-a), 13-17 June (the onset vortex formation period over the Arabian Sea, Fig. 9-b), 20-24 June (the onset period, Fig. 9-c) and 10-14 July (monsoon trough formation period in the Bay of Bengal , Fig. 9-d). For our convenience we will call the periods of 10-14 June, 13-17 June, 20-24 June and 10-14 July as the pre-onset, the vortex formation the onset and the mature phases of the monsoon respectively. The meridional profile of the mean zonal wind averaged for each time period (Fig. 9) shows the existence of a low-level jet near 6°N in the pre-onset phase. This jet shifted northward and widened with marked intensification as the monsoon progressed over the Arabian Sea and India. On the other hand, the easterlies with maximum speeds near 12° S decrease with time. The possible linkage between the intensification of westerlies in the Northern Hemisphere and the weakening of easterlies in the Southern Hemisphere and the maintenance of the westerly jet deserves a separate investigation.

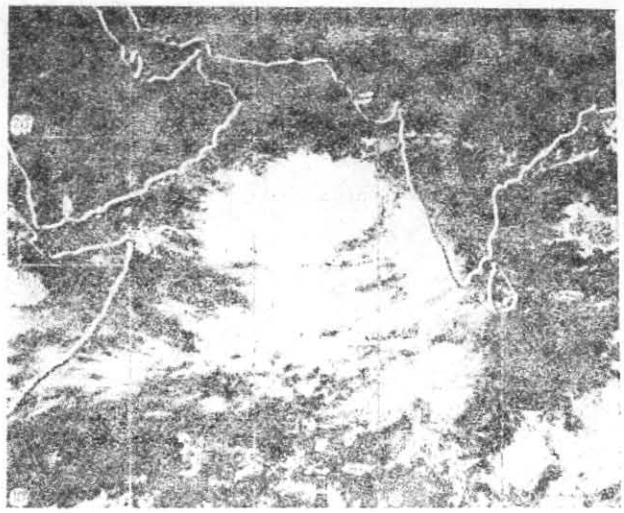

Fig. 11. DMSP satellite picture on 15 June 1979. The onset vortex is seen over the central Arabian Sea

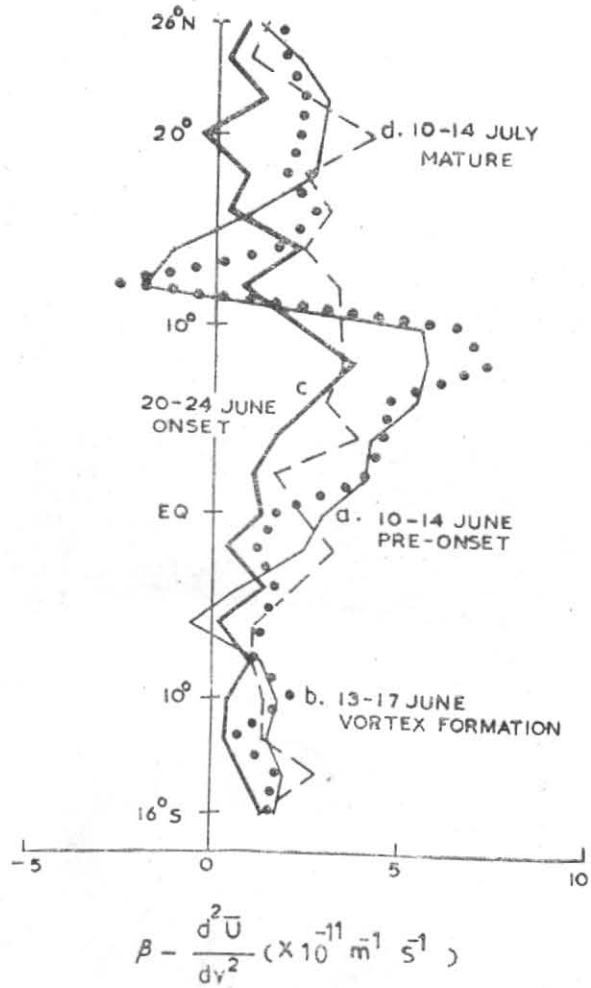

Fig. 12. The mean meridional gradient of the low-level absolute vorticity as a function of latitude for (a) the pre-onset (——), (b) the vortex formation (...), (c) the onset (——) and (d) the mature (---) phases

The corresponding upper-level mean zonal wind profiles for each phase are presented in Fig. 10. Lacking upper-level cloud tracers over the western Arabian Sea and over the Indian Ocean we have constructed only the upper-level meridional profiles of mean zonal winds between 22°N and 16°S. The profiles in Fig. 10 show the strengthening of easterlies during the pre-onset to onset phase. However, the maximum values of easterlies decrease during the mature phase (Fig. 10-d).

The onset vortex can be seen clearly from the DMSP satellite pictures (Krishnamurti *et al.* 1979). On 10 June 1979 the ITCZ extended from westnorthwest to eastsoutheast over the southern Arabian Sea (not shown here). A small convective disturbance centred at about 10°N and 60° E developed at the northwestern edge of of the ITCZ on 11 June. This disturbance moved northeastward with a phase speed of about 2 ms^{-1} until 14 June, when the disturbance was markably intensified as an onset vortex centred at about 16° N and 67° E. On 15 June the disturbance over the central Arabian Sea became nearly stationary and its horizontal scale was about 10 degrees (Fig. 11). On 17 June this system appeared to split into two systems; one moved northeastward to northern India and the other moved westward to the Arabian desert. On 19 June these systems dissipated. A strengthening of the zonal flow (and a low-level jet) over the Arabian Sea and the subsequent formation of the onset vortex suggest the possible importance of barotropic dynamics on the formation of this disturbance. The present paper is devoted to an analysis of this problem.

6. Conditions for barotropic instability

We now examine whether the necessary condition for the occurrence of barotropic instability is satisfied by the horizontally shearing mean zonal monsoon flow shown in Figs. 9 and 10. That is, does the north-south gradient of its absolute vorticity change its sign somewhere on the meridional plane (Kuo 1949, 1973) ? For this purpose we evaluate $\frac{d}{dy}\left(f-\frac{d\bar{u}}{dy}\right)$ where $\bar{u}$ is the time and zonal mean wind, using mean zonal wind profiles in Fig. 9 and present the result in Fig. 12. The pre-onset phase (Fig. 12-a) and the vortex formation phase (Fig. 12-b) satisfy the necessary condition for barotropic instability at different latitudes. However, the onset phase (Fig. 12-c) barely satisfies the condition at around 20° N. The mature phase (Fig. 12-d) does not meet the necessary condition. On occasions cloud disturbances are seen in the Arabian Sea in the post-onset phase (for example 24 July 1979) but most of them originate in the Bay of Bengal and move into the Arabian Sea. This observational evidence coincides well with the conditions for barotropic instability in Fig. 12. None of the upper-level zonal wind profiles in Fig. 10 meets the necessary condition. This suggests that barotropic instability is only important in the developing stage of the summer monsoon and is confined to the lower troposphere. Furthermore, barotropic instability may provide the triggering machanism for the monsoonal disturbance even though it is likely that its amplification and maintenance are associated with other mechanisms such as latent heat and/or baroclinic instability.

7. Numerical method for the barotropic model

In section 3 we noted that the maximum meridional wind is confined to the west of 50°E along the east coast of Africa (Fig. 2). Compared to the zonal wind speeds, the meridional components are much weaker in magnitude (Fig. 8) at least in the early stages of monsoon development. Based on satellite cloud pictures (not presented here) and preliminary analysis of the low level flow fields during the early stages of monsoon, it may be reasonable to assume that the zonal flow is nearly nondivergent in the study area, and that the compressibility and latent heat release are not significant.

The linearized barotropic vorticity equation relative to a rotating system is :

$$\left(\frac{\partial}{\partial t}+\bar{u}\frac{\partial}{\partial x}\right)\nabla^2\psi'+\left(\beta-\frac{d^2\bar{u}}{dy^2}\right)\frac{\partial\psi'}{\partial x}=0 \qquad (1)$$

where x and y are the Cartesian coordinates directed toward the east and north respectively, ψ' is the perturbed stream function, $\beta=\frac{\partial f}{\partial y}$ and ∇^2 is the Laplacian operator. The mean zonal current, $\bar{u}$, is a function of y only.

The linear solution for Eqn. (1) can be obtained by employing an initial value type numerical technique (Brown 1969) for a given basic wind field, zonal wavelength, and an initial guess of the perturbation stream function. In this study we employ the conventional numerical approach followed by Haltiner (1963) to find the characteristic value of the phase velocity C.

The harmonic wave solution of Eqn. (1) is assumed to be of the form :

$$\psi'(x, y, t)=\psi(y)\,e^{ik(x-Ct)} \qquad (2)$$

where the phase velocity C ($\equiv C_r+iC_i$) and the perturbation amplitude $\psi(y)$ are complex variables and k is the real zonal wave number. Substituting Eqn. (2) into Egn. (1) yields :

$$\left(\bar{u}-C\right)\left(\frac{d^2\psi}{dy^2}-k^2\psi\right)+\left(\beta-\frac{d^2\bar{u}}{dy^2}\right)\psi=0 \qquad (3)$$

For boundary conditions it will be assumed that $\psi(y)=0$ at the northern (28° N) and southern boundaries (18° S).

Use of the usual centred difference approximations for the derivatives in Eqn. (3) results in the following system :

$$\frac{u_i-C}{d^2}\left(\psi_{i+1}+\psi_{i-1}-2\psi_i\right)+$$

$$+\left[k^2C-k^2u_i+\beta_i-\left(\frac{\bar{u}_{i+1}+\bar{u}_{i-1}-2\bar{u}_i}{d^2}\right)\right]\psi_i=0$$

where d is the meridional grid distance (2°). Rearranging the above differential equation yields a generalized eigenvalue problem :

$$(\mathbf{A}-C\,\mathbf{B})\psi=0 \text{ or } \mathbf{A}\,\mathbf{B}^{-1}\psi=C\psi \qquad (4)$$

where **A** and **B** are square tridiagonal matrices involving the velocity, latitude and zonal wave number and ψ is an eigenvector of $\mathbf{A}\,\mathbf{B}^{-1}$ (assuming that **B** is nonsingular). Thus the complex phase velocities are the eigenvalues.

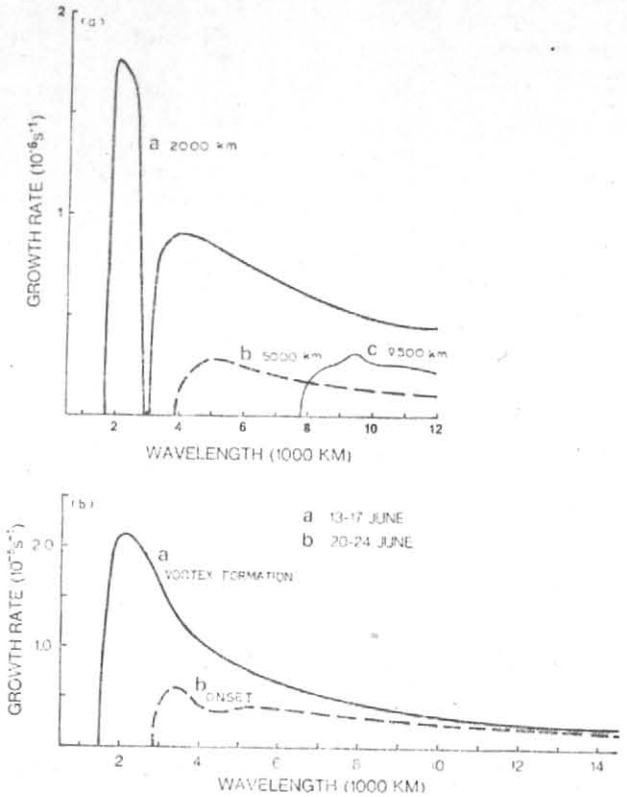

Fig. 13. The growth rate of barotropically unstable waves as a function of wavelength for (a) pre-onset and (b) onset phases: a-2000 km, b-5000 km, c-9500 km wavelength disturbances

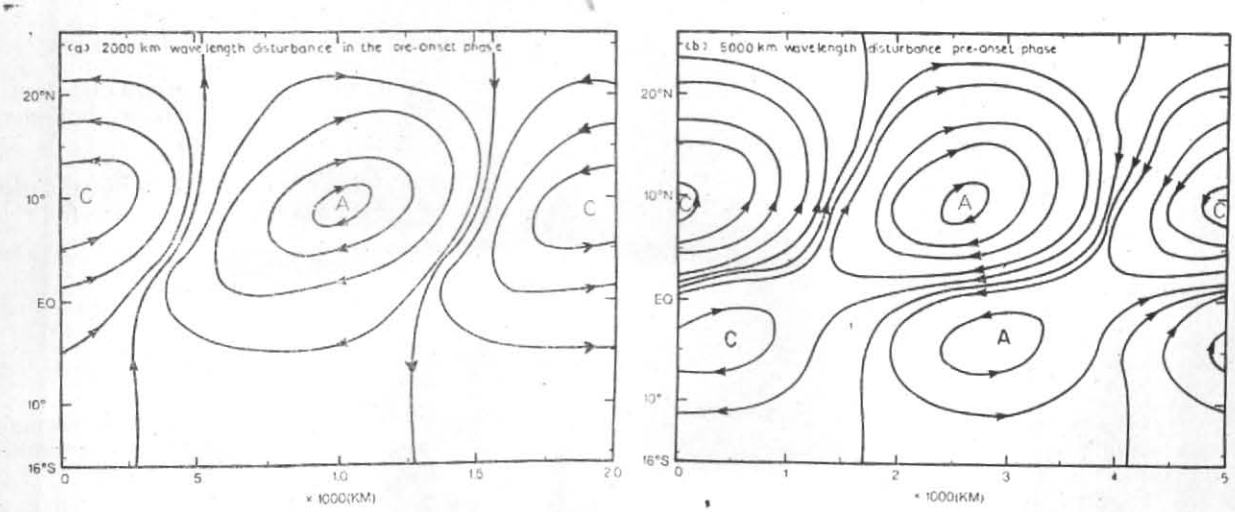

Fig. 14. The structure of perturbation stream function for (a) the 2000 km wave-length disturbance and (b) in the pre-onse phase. The letters A and C represent the centres of anticyclonic and cyclonic disturbances respectively

of the matrix $A B^{-1}$ and the amplitude functions ψ are its eigenvectors. The method to find the eigenvalues and the corresponding eigenvectors is described in Wilkinson (1954), Feller and Forsythe (1951) and Osborne (1958) etc.

8. Numerical results

The five-day averaged mean zonal wind profiles shown in Fig. 9 which satisfy the condition for barotropic instability have been investigated to determine phase velocities (C_r) and growth rates (kC_i)$^{-1}$ for various zonal wavelengths. Figs. 13(a) & 13(b) show the growth rates of various wavelengths for the pre-onset (10-14 June), the vortex formation (13-17 June) and the onset phases (20-24 June). The pre-onset phase [Fig. 13(a)] shows several unstable wave modes. The most unstable mode (wavelength$\simeq$2000 km) has an eastward propagation speed of about 3.6 ms^{-1} with a maximum growth rate of 1.78×10^{-6}s^{-1} which corresponds to an *e*-folding time 6.5 days. The growth rate of 3000 km wavelength is too small to be sown in Fig. 13(a)-a. However, there is no discontinuity of the growth rate in this wavelength. The other unstable modes have much smaller growth rates. For example, the 5000 km mode has a growth rate of 0.27×10^{-6} s^{-1} (*e*-folding time $\simeq$42 days) and propagates eastward with a phase velocity of 1.6 ms^{-1}. Another is the Rossby wave propagating westward with a phase velocity of -5.8 m s^{-1}, and a maximum growth rate of $.33\times10^{-6}$ s^{-1} (*e*-folding time $\simeq$35 days) at wavelength 9500 km. However, these two unstable modes may not be physically significant partly because of their smaller growth rates and partly because of the basic zonal wind being taken over the Arabian Sea which is smaller than one wavelength of the latter unstable mode. During the vortex formation phase [Fig. 13(b)-a] the multimode of unstable waves in the pre-onset phase disappears, and one dominant mode is intensified. This wave disturbance has a wavelength of 2000 km and an eastward propagation speed of about 5.6 ms^{-1} with the maximum growth rate of 2.12×10^{-6} s^{-1} (*e*-folding time $\simeq$5.5 days).

The scale of onset vortex described in Section 5 corresponds closely to that implied by the barotropic stability analysis during the vortex formation phase. However, the phase speed obtained by the barotropic analysis (3.6-5.6 m s^{-1}) is slightly larger than that of the observation. A significant reduction of the growth rate during the onset phase [Fig. 13(b)-b] and the disappearance of the unstable wave during the mature phase clearly indicate that the barotropic instability no longer plays any significant role in the monsoon circulation during the onset and the post-onset periods over the Arabian Sea. During the early phase of monsoon onset over the Arabian Sea, eddy motions periodically grow at the expense of mean zonal kinetic energy with a period of about 5-6 days as implied by the above barotropic analysis during the vortex formtion period. The period of such energy exchange is found to be similar to that estimated by Charney (1959) and Wiin-Nielsen (1961).

The disturbance stream functions for those unstable modes in the pre-onset phase are shown in Fig. 14. The coordinates cover one wavelength in x and various latitudes varying from 26°N to 16°S with 2° intervals in y. The streamlines are drawn at equal intervals on an arbitrary scale. The maximum amplitude of the disturbance for a wavelength of 2000 km (Fig. 14 a) occurs near 10°N, which is the northern flank of the low-level westerly jet centred at about 6°N and also well coincides with the location of the observed initial disturbance. The letters A and C represent the primary centres of anticyclonic and cylonic circulation. The waves have a southwest-northwest orientation, which implies a northward transport of zonal momentum. The growing wave obtains its kinetic energy at the expense of the zonal mean kinetic energy through barotropic instability.

The perturbation stream function for the 5000 km wavelength unstable mode is depicted in Fig. 14 (b). This unstable mode has two maxima; the major disturbance occurs at about 10° N as in the case of the 2000 km wavelength mode, and the other secondary disturbance near 4° S; this corresponds to the condition of barotropic instability in Fig. 12-a. The wave tilting is more pronounced than that of the 2000 km scale mode. In the vortex formation phase, the perturbation stream function (Fig. 15) for the most unstable wave (wavelength 2000 km) resembles the 2000 km wave in the pre-onset phase except that the tilting of the axis of the wave is more pronounced in the vortex formation phase than in the pre-onset phase. This gives an increased northward transfer of momentum.

The structure of the onset phase barotropic disturbance in Fig. 16 shows a slight tilt from southwest to northeast, suggesting a weakening of the northward transfer of momentum. The disappearance of unstable barotropic wave in the mature phase and the gradual reduction of the growth rate from the vortex formation to the onset phase clearly suggest that barotropic instability is only important in the early onset-phase of the summer monsoon over the Arabian Sea. This finding agrees with the observational fact that cyclogenesis of active monsoon disturbances over the Arabian Sea during the post-onset period is a rare event (Krishnamurti *et al.* 1981). However, Krishnamurti *et al.* (1981) showed that a strong barotropic energy exchange from zonal to eddy motion occurs during the post-onset phase, in which period we find no barotropic instability anywhere over the Arabian Sea. Their strong barotropic energy exchange might have resulted from improper time averaging as well as small domain (20 longitude span over the Arabian Sea) averaging in the calculation of the growth rate of barotropically unstable disturbances.

The average net momentum transfer function (*see* Kuo 1973; Pedlosky 1979, p. 506) is given by :

$$-\frac{d}{dy}\overline{(u'v')} = -\frac{kC_i}{2}|\psi|^2\frac{\beta-\frac{d^2\bar{u}}{dy^2}}{|\bar{u}-C|^2}e^{2kc_it} \qquad (5)$$

where ψ is the complex variables of the perturbation ampliudte of the stream function.

The average net momentum transfer function for the most dominant unstable modes, normalized by their maximum values, is plotted in Figs. 17 and 18 for the

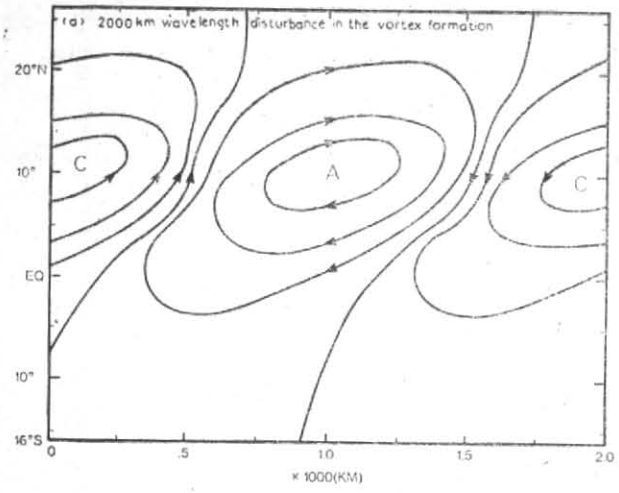

Fig. 15. The structure of perturbation function for the 2000 km wavelength disturbance in the vortex formation phase

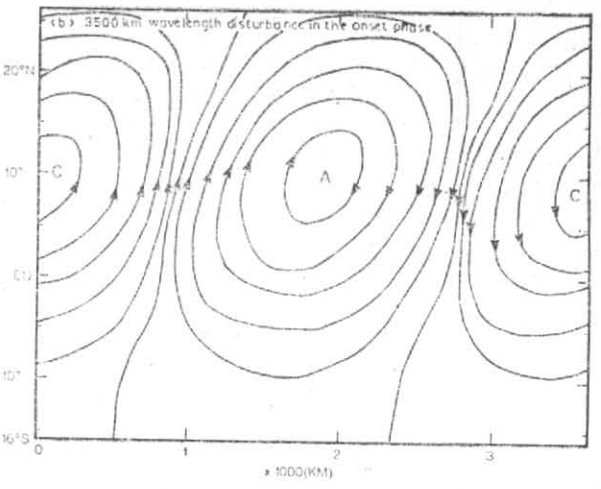

Fig. 16. The structure of perturbation function for the 3500 km wavelength disturbance in the onset phase

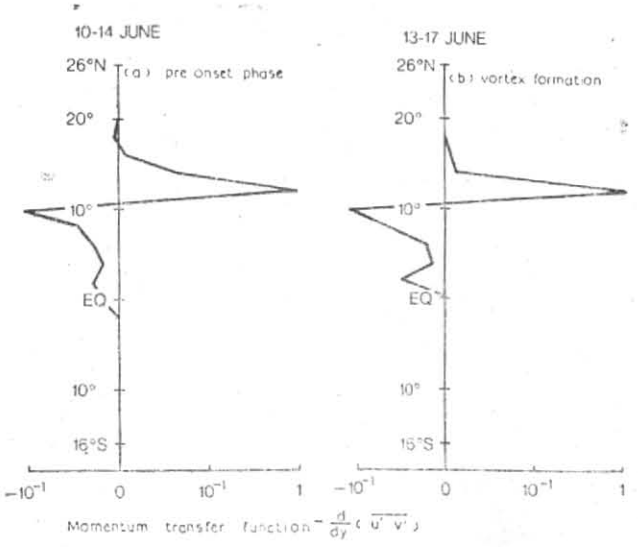

Fig. 17 Fig. 18

Figs. 17 & 18. Average net momentum transfer function $\left[(-\frac{d}{dy}(\overline{u'v'})\right]$ as a function of latitude for the 2000 km wavelength disturbance in the pre-onset phase (Fig. 17) & in the vortex formation phase (Fig. 18)

pre-onset and the vortex formation phases. The momentum transfer function for the 2000 km disturbance in the pre-onset phase (Fig. 17) is negative in the maximum shear zone and the jet axis, and is positive just north of the maximum cyclonic shear zone. Those profiles associated with the other two unstable modes (5000 km wavelength) shown in Fig. 13(b) -b in the pre-onset phase and in the onset phase in Fig. 16 are not shown here since the growth rates of these disturbances are too small to allow the disturbances to grow against the frictional dissipation in the lower atmosphere. Their contribution to the monsoon circulation is of no significance. Fig. 18 shows the normalized average momentum transfer profile of the 2000 km wavelength in the vortex formation phase. The pattern of the momentum transfer associated with this disturbance is similar to that of the 2000 km wave disturbance in the pre-onset phase with a maximum positive value just north of the maximum shear zone. The above computations imply that the momentum transfer associated with wave disturbances reduces the maximum shear in the shear zone and intensifies the disturbances at the expense of the zonal kinetic energy. Furthermore, the net gain of the momentum $\left(-\frac{d}{dy}\overline{(u'v')} > 0\right)$ just north of the maximum shear zone causes the acceleration of the mean zonal wind $\left(i.e., \frac{d\bar{u}}{dt} > 0\right)$, which leads to the northward progression and the broadening of the jet axis with time. The broadening of the low-level jet implies the reduction of the horizontal wind shear. This, in turn, reduces barotropic instability.

9. Summary and conclusions

In this paper we have studied the dynamical features in the early stages of the summer monsoon circulation over the Arabian Sea using daily low-level and upper-level satellite wind fields.

The monsoon circulation starts with the intensification of both zonal and meridional winds over the Arabian Sea and progresses northward in time beginning at the equator around 10 June. During 10-14 June the low level jet (Somali jet) is formed over the Arabian Sea with its axis near 6°N. A numerical barotropic stability analysis shows that this low-level jet profile exhibits a multimode of unstable barotropic wave disturbances. The wavelength of the most unstable wave is 2000 km with *e*-folding times 6.5 days. The amplification rate of other disturbance appeared in the barotropic stability analysis with wavelengths of 5000 km is not large enough to allow a small disturbance to overcome the effects of friction in the atmosphere, while the dominant mode with wavelength 2000 km persists and intensifies during the vortex formation phase. The growth of this barotropic wave disturbance is manifested in the observed onset vortex over the Arabian Sea centred at about 15° N.

The structure of this disturbance is tilted southwest to northeast implying a northward transport of zonal momentum from the maximum cyclonic shear zone to further northward, causing an acceleration of the mean zonal wind to the north. Consequently the low-level jet becomes broader with a reduced wind shear. The broadening of the jet is attributed partly to the barotropic wave disturbance over the Arabian Sea. Two significant dynamical consequences follows : (*a*) the region becomes barotropically less unstable due to the reduction of the horizontal wind shear, and (*b*) the east-west monsoonal circulation is accelerated by the rising motion over the Indian subcontinent and the sinking motion over the western Arabian Sea and the Arabian desert due to the horizontal differential advection. The rare occurrence of cyclogenesis over the Arabian Sea during the post-onset phase can be explained, at least partially, by the reduction of the barotropic instability and the enhanced sinking motion associated with the monsoon circulation.

The present study has provided strong evidence of the importance of barotropic dynamics in the early stages of the mean zonal monsoon current over the Arabian Sea. In the mature phase, the Arabian Sea region is barotropically stable. This is expected because in the mature phase of the Indian monsoon, Bay of Bengal depresions account for a majority of the rainfall over the subcontinent and for the intensification of zonal flow over the Arabian Sea. This study also suggests that the satellite derived wind field could be used quantitatively to analyze dynamic stability of the atmosphere.

Acknowledgements

The authors wish to thank Drs. David W. Martin and Jan-Hwa Chu of Space Science and Engineering Center, University of Wisconsin at Madison for many helpful discussions. Thanks are also extended to Donna Bobst for typing the manuscript, and to Donna Genzmer for drafting the figures. This research was supported by the GARP office, National Science Foundation through grant No. ATM 7920850 and the Graduate School

University of Wisconsin at Milwaukee. A part of the computer funds came from the College of Letters and Science, University of Wisconsin at Milwaukee.

References

Bates, J.R., 1970, 'Dynamics of disturbances on the intertropical convergence zone', *Quart. J. R. met. Soc.*, **96**, 677-701.

Brown, J.A., 1969, 'A numerical investigation of hydrodynamic instability and energy conversions in the quasi-geostrophic atmosphere' : Part I, *J. atmos. Sci.*, **26**, 352-365.

Charney, J., 1959, 'On the general circulation of the atmosphere', *The Atmosphere and the Sea in Motion*, Rossby memorial Volume, Rockefeller Institute Press, New York, 178-193.

Charney, J., 1963, 'A note on large-scale motions in the tropics', *J. atmos. Sci.*, **20**, 607-609.

Charney, J. and Eliassen, A., 1949, 'A numerical method of predicting the perturbations of the middle latitude westerlies', *Tellus*, **1**, 38-54.

Charney, J. and Eliassen, A., 1964, 'On the growth of the hurricane depression', *J. atmos. Sci.*, **21**, 68-75.

Eliasen, E., 1954, 'Numerical solutions of the perturbation equation for linear flow', *Tellus*, **6**, 183-192.

Endlich, R.M. and Mancuso, R.L., 1968, 'Objective analysis of environmental conditions associated with severe thunderstorms and tornadoes', *Mon. Weath. Rev.*, **96**, 342-350.

Feller, W. and Forsythe, G.E., 1951, 'New matrix transformations for obtaining characteristic vectors', *Quart. Appl. Math.*, **8**, 325-331.

Haltiner, G.J., 1963, 'Finite difference approximations for the determination of dynamic instability', *Tellus*, **15**, 230-240.

Holton, J.R., 1972, '*An introduction to dynamic meteorology*, Academic Press, New York and London, 319 pp.

Krishnamurti, T.N., Ardanuy, P., Ramanathan, Y. and Pasch, R., 1981, 'On the onset vortex of the summer monsoon', *Mon. Weath. Rev.*, **109**, 344-363.

Krishnamurti, T.N., Ardanuy, P., Ramanathan, Y. and Pasch, R., 1979, 'Quick look *'summer MONEX atlas'* Part *V*: *The onset phase*, Department of Met., Florida State Univ., Tallahassee, FL 32301, 205 pp.

Kuo, H.L., 1949, 'Dynamic instability of two-dimensional nondivergent flow in a barotropic atmosphere', *J. Met.*, **6**, 105-122.

Kuo, H.L., 1965, 'On formation and intensification of tropical cyclones through latent heat release by cumulus convection', *J. atmos. Sci.*, **22**, 40-63.

Kuo, H.L., 1973, Dynamics of quasigeostrophic flows and instability theory, *Advances Appl. Mech.*, **13**, 247-331.

Lipps, F.B., 1962, The barotropic stability of the mean winds in the atmosphere, *J. Fluid Mech.*, **12**, 397-407.

Lipps, F.B., 1965, The stability of an asymmetric zonal current in the atmosphere, *J. Fluid Mech.*, **21**, 225-239.

Osborne, E.E., 1958, On acceleration and matrix deflation processes used with the power method, *J. Soc. Indust. Appl. Math.*, **6**, 279-287.

Pedlosky, J., 1979, *Geophysical Fluid Dynamics*, Springer-Verlag, New York, Heidelberg Berlin, 624 pp.

Riehl, H., 1948, 'On the formation of typhoons', *J. Met.*, **5**, 247-264.

Shukla, J., 1978, 'CISK-barotropic-baroclinic instability and the growth of monsoon depressions', *J. atmos. Sci.*, **35**, 495-508.

Wiin-Nielsen, A., 1961, 'On short and long-term variations in quasi-barotropic flow', *Mon. Weath. Rev.*, **89**, 461-476.

Wilkinson, J.H., 1954, 'The calculation of the latent roots and vectors of matrices on the pilot model of the A.C.E.', *Proc. Cambridge Philos. Soc.*, **50**, 536-566.

Williams, R.T., Schminke, T.K. and Newman, R.L., 1971, 'Effect of surface friction on the structure of barotropically unstable tropical disturbances', *Mon. Weath. Rev.*, **99**, 778-785.

Yamasaki, M., 1969, 'Large-scale disturbances in a conditionally unstable atmosphere in low latitudes', *Papers Meteor. Geophys.*, Tokyo, **20**, 289-336.

Yanai, M. and Nitta, T., 1968, 'Finite difference approximations for the barotropic instability problem', *J. met. Soc. Japan*, **46**, 389-403.

Young, J., Virgi, H., D.P., Wylie and Lo, C., 1980, 'Summer monsoon windsets from geostationary satellite data', Space Science Engineering Center and Department of Met., Uni. of Wisconsin-Madison, 127 pp.